Proton Plasma Asymmetries between Venus' Quasi-Perpendicular and Quasi-Parallel Magnetosheaths

Sebastián Rojas Mata[1], Gabriella Stenberg Wieser[1], Yoshifumi Futaana[1], and Tielong Zhang[2]

[1]Swedish Institute of Space Physics
[2]Space Research Institute Austrian Academy of Sciences

December 7, 2022

Abstract

Proton plasma asymmetries between the hemispheres of Venus' dayside magnetosheath lying downstream of the quasi-perpendicular ($q_\perp$) and quasi-parallel ($q_\parallel$) sides of the bow shock are characterized using measurements taken by a mass-energy spectrometer. This characterization enables comparison to analogous Earth studies, thereby providing insight as to which plasma phenomena, such as turbulent particle heating, contribute in creating the observed plasma asymmetries in planetary magnetosheaths. A database of dayside bow-shock crossings along with magnetosheath proton densities, bulk speeds, temperatures, and magnetic-field strengths is manually constructed by selecting measurements taken during stable solar-wind conditions. Ratios of these magnetosheath proton parameters are calculated as functions of distance from the central meridian and the upstream Alfvén Mach number to quantify the $q_{\perp/\parallel}$ asymmetries. The density and bulk-speed exhibit $q_\parallel$-favored asymmetries, mirroring those observed at Earth, whereas the magnetic-field strength reveals no significant asymmetry despite expectations based on simulations. The temperatures perpendicular ($T_\perp$) and parallel ($T_\parallel$) to the background magnetic field have $q_\perp$-favored asymmetries while the temperature anisotropy $T_\perp / T_\parallel$ exhibits a $q_\parallel$-favored asymmetry. This trend is opposite to that seen at Earth, suggesting that the different spatial scales of the two planets' magnetosheaths may affect the impact of turbulent processes on global plasma properties.

Proton Plasma Asymmetries between Venus' Quasi-Perpendicular and Quasi-Parallel Magnetosheaths

Sebastián Rojas Mata[1], Gabriella Stenberg Wieser[1], Yoshifumi Futaana[1], and Tielong Zhang[2]

[1]Swedish Institute of Space Physics, Kiruna, Sweden
[2]Space Research Institute, Austrian Academy of Science, Graz, Austria

Key Points:

- We compile a database of dayside bow-shock crossings and proton plasma parameters measured in Venus' dayside magnetosheath
- We characterize plasma asymmetries between the quasi-perpendicular/parallel magnetosheaths as functions of longitude and Alfvén Mach number
- Proton temperatures and temperature anisotropies are higher downstream of the quasi-parallel bow shock, contrasting with Earth observations

Corresponding author: Sebastián Rojas Mata, sebastian.rojasmata@irf.se

Abstract

Proton plasma asymmetries between the hemispheres of Venus' dayside magnetosheath lying downstream of the quasi-perpendicular ($q_\perp$) and quasi-parallel ($q_\parallel$) sides of the bow shock are characterized using measurements taken by a mass-energy spectrometer. This characterization enables comparison to analogous Earth studies, thereby providing insight as to which plasma phenomena, such as turbulent particle heating, contribute in creating the observed plasma asymmetries in planetary magnetosheaths. A database of dayside bow-shock crossings along with magnetosheath proton densities, bulk speeds, temperatures, and magnetic-field strengths is manually constructed by selecting measurements taken during stable solar-wind conditions. Ratios of these magnetosheath proton parameters are calculated as functions of distance from the central meridian and the upstream Alfvén Mach number to quantify the $q_{\perp/\parallel}$ asymmetries. The density and bulk-speed exhibit $q_\parallel$-favored asymmetries, mirroring those observed at Earth, whereas the magnetic-field strength reveals no significant asymmetry despite expectations based on simulations. The temperatures perpendicular ($T_\perp$) and parallel ($T_\parallel$) to the background magnetic field have $q_\perp$-favored asymmetries while the temperature anisotropy $T_\perp/T_\parallel$ exhibits a $q_\parallel$-favored asymmetry. This trend is opposite to that seen at Earth, suggesting that the different spatial scales of the two planets' magnetosheaths may affect the impact of turbulent processes on global plasma properties.

1 Introduction

Planetary magnetosheaths serve as intermediary regions through which the solar wind transfers momentum and energy to a planet's magnetosphere (Longmore et al., 2005; Haaland et al., 2017; Turc et al., 2020). Understanding this dynamic plasma environment contributes to studies of fundamental concepts such as plasma boundary morphology (Slavin & Holzer, 1981; Spreiter & Stahara, 1994), wave phenomena (Dimmock, Osmane, et al., 2015; Soucek et al., 2015; Sundberg, 2017; Jin et al., 2022), or particle dynamics (Richardson, 2002; Halekas et al., 2017), as well as to applied endeavors like space weather forecasting (Stahara, 2002; Lapenta et al., 2013). Over decades, plasma data provided by spacecraft has continuously renewed our understanding of magnetosheath physics, for example by extending models from (magneto)hydrodynamic (Spreiter & Alksne, 1966; Spreiter & Stahara, 1980, 1994; Stahara, 2002) to kinetic (Kallio et al., 2011; Karimabadi et al., 2014; Jarvinen et al., 2016; Modolo et al., 2018; Palmroth et al., 2018;

Turc et al., 2020) approaches, especially as new features of planetary magnetosheaths are uncovered.

At Earth, one such distinctive feature is that the magnetosheath plasma is not axisymmetric about the axis parallel to the upstream solar-wind velocity. Particularly, notable differences in plasma parameters exist between the pre-noon and post-noon (alternatively, west and east or dawn and dusk) hemispheres. These asymmetries involve local plasma parameters like density, temperature, or magnetic field (Paularena et al., 2001; Němeček et al., 2002; Longmore et al., 2005; B. M. Walsh et al., 2012; Dimmock & Nykyri, 2013; A. P. Walsh et al., 2014; Dimmock, Osmane, et al., 2015) and influence many plasma processes and structures (see A. P. Walsh et al. (2014) or Haaland et al. (2017) for broad reviews). Though certain upstream conditions (e.g. the orientation of the IMF) partly explain some asymmetries (e.g. the thicker magnetosheath in the dusk hemisphere (A. P. Walsh et al., 2014)), the causes for many of them remain under debate (B. M. Walsh et al., 2012; Dimmock & Nykyri, 2013; Dimmock, Nykyri, et al., 2015; A. P. Walsh et al., 2014; Haaland et al., 2017).

Data-based investigations of similar asymmetries at other planets' magnetosheaths are unfortunately scarcer, thus limiting possible comparative analyses. Jupiter and Saturn exhibit dawn-dusk asymmetries involving plasma flows, magnetic fields, and aurora (Palmaerts et al., 2017; Carbary et al., 2017). While some of these asymmetries are Earth-like, these planets' rotationally driven magnetospheres, which contain significant internal sources of particles (Io and Enceladus, respectively), include non-Earthlike characteristics which complicate the comparison (Palmaerts et al., 2017; Carbary et al., 2017). Dawn-dusk asymmetries of plasma fluxes have also been observed at Mars (Kallio et al., 1994; Dubinin et al., 2008), however many studies focus on north-south asymmetries (Wang et al., 2020; Romanelli et al., 2020) or on the ionosphere/atmosphere (Dubinin et al., 2012; Andrews et al., 2013; Gupta et al., 2019), so there is limited work for comparison.

Luckily, Venus is a "potentially useful space plasma 'laboratory' experiment for magnetosheath studies," particularly due to its many similarities with Earth (e.g. size and distance from the Sun) (Luhmann, 1995). Since it does not have an intrinsic magnetic field, its induced magnetosheath is much smaller than Earth's (Futaana et al., 2017), making it more likely that spacecraft can traverse the magnetosheath under constant upstream conditions (Luhmann, 1995). Though previous studies at Venus have investigated hemispherical asymmetries in boundary locations (Phillips et al., 1988; Zhang, Luhmann, & Russell, 1991; Zhang, Schwingenschuh, et al., 1991; Chai et al., 2015), magnetic-field structures (Du et al., 2013; Delva et al., 2017; Xiao et al., 2018), or pick-up ion dynamics (Phillips et al., 1987; Barabash, Fedorov, et al., 2007), none provided statistical characterizations of the magnetosheath plasma analogous to those available at magnetized planets. Recent studies investigating solar-cycle dependencies of Venus' plasma environment found no noticeable spatial asymmetries in plasma parameters in the magnetosheath (Bader et al., 2019; Rojas Mata et al., 2022), however these were coarse statistical studies in a reference frame in which existing asymmetries may be obscured.

In this paper we characterize the proton plasma asymmetries between the two hemispheres of Venus' dayside magnetosheath lying downstream of the quasi-perpendicular ($q_\perp$) and quasi-parallel ($q_\|$) sides of the bow shock. We refer to these regions as the $q_\perp$ and $q_\|$ magnetosheaths, which at magnetized planets statistically correspond to the dawnside and duskside hemispheres of the magnetosheath. We first overview in Section 2 the ion instrument and specialized data set compiled for this study. The details of our methodology for quantifying parameter asymmetries in a frame defined by solar-wind electromagnetic-field configurations and bow-shock geometry follow in Section 3. We present our results in Section 4 and discuss their implications on our understanding of Venus and Earth's magnetosheaths in Section 5. Concluding remarks in Section 6 provide a summary of the work and future research directions.

2 Proton Plasma Measurements and Dayside Magnetosheath Database

The Earth studies mentioned above propagate measurements from an upstream monitor (such as OMNI or ACE, see https://omniweb.gsfc.nasa.gov/) to determine the solar wind conditions associated with spacecrafts' magnetosheath measurements. Our analysis uses data taken by the Venus Express (VEX) mission (Svedhem et al., 2007), a single-spacecraft mission with no dedicated upstream monitor, so it must serve as its own solar-wind monitor. Conveniently, the small scale of Venus' magnetosheath allowed VEX to observe the solar wind during extended portions of each orbit. To properly use VEX as a solar-wind monitor requires careful filtering of the data to ensure that we only include orbits which have well-defined upstream conditions. In this section we overview the general plasma measurements available and then detail the procedure for compiling a subset of dayside magnetosheath measurements with well-defined upstream conditions.

2.1 Ion Mass-Energy Spectrometer

We use data collected by the Ion Mass Analyser (IMA) instrument, a cylindrically symmetric ion mass-energy spectrometer which was part of the Analyser of Space Plasmas and Energetic Atoms (ASPERA-4) experiment on board VEX (Barabash, Sauvaud, et al., 2007). The instrument had 32 mass-per-charge channels (moderate mass resolution of $M/dM \gtrsim 1$ up to 80 amu/q), 96 logarithmic energy-per-charge steps ($\sim$0.01–30 keV/q), and 16 azimuth $\times$ 16 elevation angles. Measuring particle counts over the pixels of this mass-energy-azimuth-elevation parameter space took 192 s and spanned a 360°×90° field of view. We use mass-separated data from the entire mission (2006–2014) and concentrate on protons. We note that the instrument does not differentiate between solar-wind and planetary protons. Concurrent 1-second-resolution magnetic-field-vector measurements taken by the VEX Magnetometer (MAG) (Zhang et al., 2006) complement the IMA data.

2.2 Proton Bulk Parameters

To calculate proton densities n, bulk velocities $\mathbf{v}$, and perpendicular/parallel temperatures $T_\perp/T_\parallel$ we use the methodology developed by Bader et al. (2019) and applied to the entire VEX data set by Rojas Mata et al. (2022). This methodology fits Maxwellian models to IMA's velocity-distribution-function (VDF) measurements and assesses the success of the fit through various goodness-of-fit criteria. We refer the reader to the extended discussion in Rojas Mata et al. (2022) for further details (including advantages and disadvantages compared to taking velocity-space moments). We only include parameters from the scans for which the fitting methodology was successful. However, in this paper we replace the densities with those calculated by taking the zeroth velocity moment (Fränz et al., 2006). In the solar wind, the narrow velocity-space spread of the particle measurements causes the Maxwellian fits to overestimate the plasma density, so the velocity-moment value is more adequate to use. In other regions, like the magnetosheath or magnetotail, we do not find significant differences between the two methods due to the particle measurements' broader energy spectrum.

2.3 Dayside Bow-Shock Crossings and Magnetosheath Scan Identification

Bader et al. (2019) and Rojas Mata et al. (2022) used average bow-shock models to determine to which spatial region (solar wind or magnetosheath) a given IMA scan belongs. This method sometimes classifies a scan incorrectly since the models do not account for the bow shock's dynamic location or asymmetry (Russell et al., 1988; Chai et al., 2015). The authors mitigated this problem by (1) excluding scans too close to the model bow shock and (2) defining a near-subsolar magnetosheath region from hand-selected bins. While this strategy sufficed then, in our present work we wish to improve the classification of the scans to better characterize the dayside magnetosheath and the solar wind, especially to use VEX as its own upstream monitor.

To this end we manually search through the entire mission data to select orbits with (1) an identifiable dayside bow-shock crossing and (2) adequate data coverage both in the solar wind and dayside magnetosheath. Identifiable bow-shock crossings are characterized by a sharp jump in the magnitude of the magnetic field (compression) and a broadening of the particle energy spectrum (particle heating). We do not locate a lower boundary for the magnetosheath (e.g. the ion composition or induced magnetosphere boundary) in this study and instead use models (Phillips et al., 1988; Martinecz et al., 2008) to set a reasonable lowest altitude of 0.2 R_V ($\sim$1200 km). We also set a highest altitude of 0.5 R_V ($\sim$3000 km) to remove outlying orbits for which the bow shock was unusually far from the planet. This initial filtering yields 817 orbits, each with 1–3 magnetosheath scans and up to 20 solar-wind scans.

2.4 Upstream Solar Wind Conditions

We next examine these orbits' solar-wind measurements to select those with well-defined upstream interplanetary magnetic field (IMF) and proton parameters. One method to assess the IMF's stability involves comparing the IMF before and after the inbound and outbound bow-shock crossings, respectively. Quantitative criteria, such as not allowing more than a 10° rotation between the average fields, then determine which orbits have a stable IMF (e.g., Masunaga et al. (2011)). While such approaches are appropriate for large-scale analyses of data from the entire time VEX was inside Venus' bow shock (up to 3 h), our study only includes 1–3 magnetosheath scans per orbit, all of which were taken $\lesssim$ 10 min downstream of the bow-shock crossing. So even though magnetosheath plasmas "respond very rapidly to changes in solar wind plasma and IMF conditions with small lagtime" (Stahara, 2002), Venus' small dayside magnetosheath enables us to implement a more localized assessment of the IMF's stability which still yields meaningful results. We therefore deem the IMF as stable if it does not exhibit strong variations in magnitude or direction during the 20-30 min immediately upstream of the bow-shock crossing. For each orbit we then calculate an average $\mathbf{B}_{IMF}$ using MAG data over a manually-defined time interval ranging 5–10 min, which suffices to average out small fluctuations.

The solar-wind proton parameters (density, speed, and temperatures) fluctuate far less than the IMF, so by simply selecting orbits with at least 4 solar-wind fits we single out those with well-defined upstream conditions. Such orbits indeed exhibit acceptably stable proton parameters as more than 80% (60%) of each orbit's solar-wind measurements deviate less than 50% (25%) from the medians. Thus, for each orbit, we assign the medians of the solar-wind measurements as the orbit's upstream solar-wind conditions. We normalize each orbit's magnetosheath parameters with their corresponding upstream medians (i.e. $\widehat{a} \equiv a/\mathrm{med}(a_{SW})$ for parameter a), thereby mitigating the variation due to the wide range of solar-wind conditions sampled (Paularena et al., 2001; Du et al., 2013).

2.5 Final Database

The above selection procedures yield a database of 1181 dayside magnetosheath scans spanning 597 orbits (i.e. 597 solar-wind conditions) (Rojas Mata & Futaana, 2022). To visualize the spatial coverage of the measurements, we first define a Cartesian Venus Solar Orbit (VSO) frame centered on Venus: $+X_{VSO}$ points from Venus' center to the Sun, $+Z_{VSO}$ is the northward normal to Venus' orbital plane, and $+Y_{VSO}$ completes the right-handed system (i.e. points antiparallel to Venus' orbital motion). We then define the VSO longitude and latitude as $\arctan(Y_{VSO}/X_{VSO})$ and $\arctan(Z_{VSO}/\sqrt{X_{VSO}^2 + Y_{VSO}^2})$, respectively. We also construct a cylindrical VSO frame by taking X_{VSO} as the axis of symmetry and collapsing the other two coordinates into the radial coordinate $R_{VSO} = \sqrt{Y_{VSO}^2 + Z_{VSO}^2}$.

We show in Figure 1 the location of the scans in the (a) cylindrical and (b) latitude-longitude VSO frames. Each marker corresponds to each scan's starting position, how-

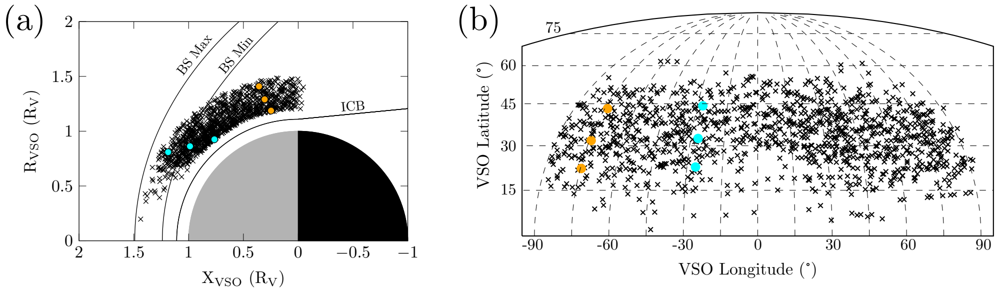

Figure 1. Spatial distribution of magnetosheath scans in (a) cylindrical and (b) latitude-longitude VSO frames. All but six scans are in the northern ($+Z_{VSO}$) hemisphere; the exceptions lie in the terminator plane. The orange and aqua markers correspond to orbits 958 and 1039, respectively. Panel (a) includes bow-shock models for solar maximum (Russell et al., 1988) and minimum (Whittaker et al., 2010) along with an ion composition boundary model (Martinecz et al., 2008).

ever IMA's 192-s cadence means in reality that a scan spans 0.2–0.3 R_V (based on spacecraft speeds of 6–10 km/s near pericenter (Titov et al., 2006)). We illustrate this by highlighting the location of the start of three consecutive scans from two different orbits (958 and 1039); each scan corresponds to an average measurement along the line joining the markers. Note that VEX's highly inclined elliptical orbits with pericenter altitudes of $160-250$ km, chosen for a variety of atmospheric experiments (Müller-Wodarg et al., 2006; Limaye et al., 2017), caused the scans to concentrate in the northern hemisphere below 60° latitude.

In Figure 2 we compare the distributions of our database's solar-wind parameters to those of the entire VEX mission. Since there is no available database of dayside bow-shock crossings for all VEX orbits we use the model-based classification of Bader et al. (2019) and Rojas Mata et al. (2022) to roughly identify solar-wind scans for all orbits. Overall the distributions agree except for our database's bias towards higher densities and the consequent bias towards higher Alfvén Mach numbers $M_A = \|\mathbf{v}\|/v_A$, where $v_A = \|\mathbf{B}\|/\sqrt{\mu_0 n m_i}$ is the Alfvén speed. This bias is reasonable as higher solar-wind densities lead to higher magnetosheath densities and therefore measurements with higher likelihoods of being successfully fit. The distribution for Parker spiral angles ϕ_P is also slightly

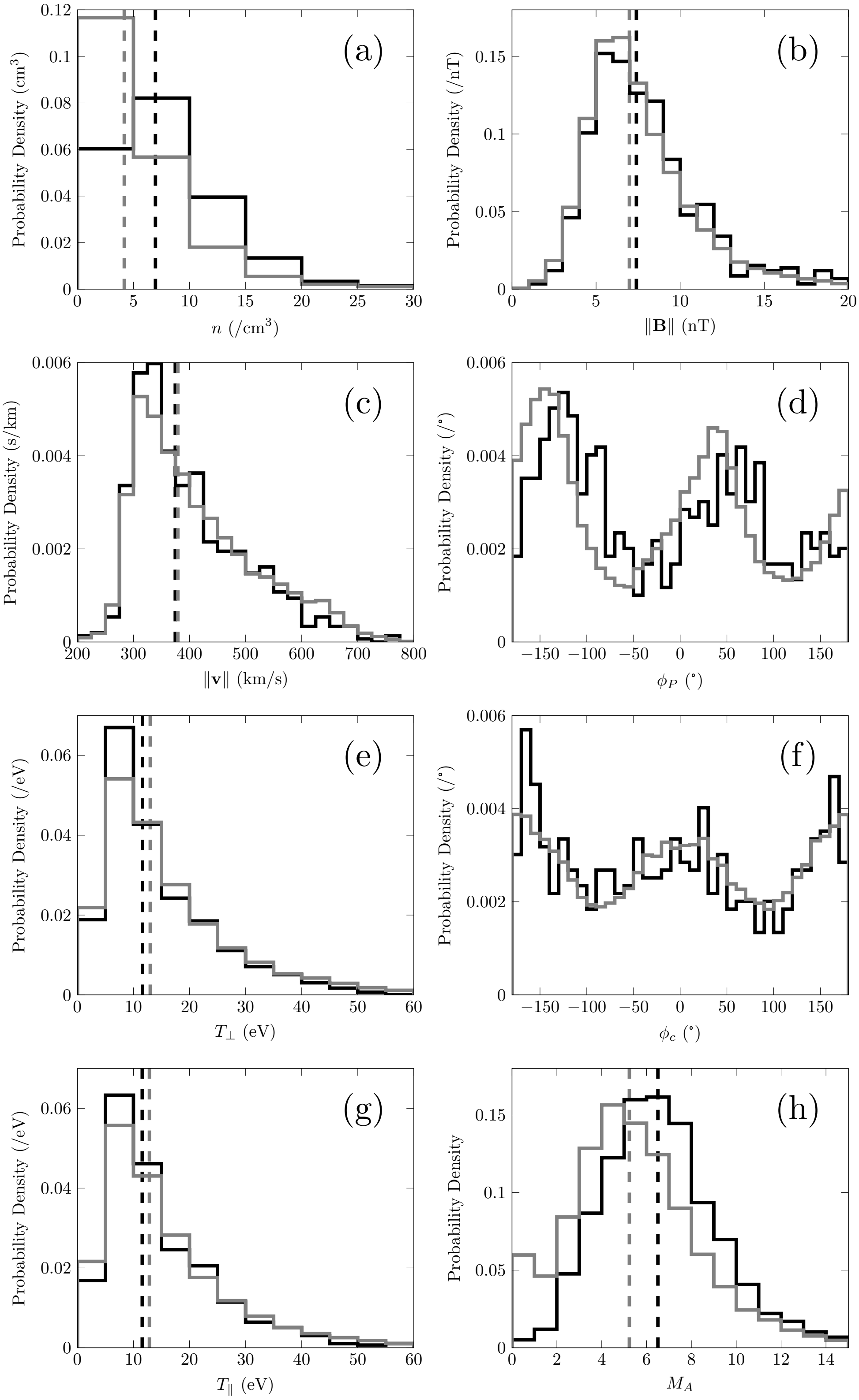

Figure 2. Comparison of solar-wind density n, speed $\|\mathbf{v}\|$, perpendicular temperature $T_\perp$, parallel temperature $T_\parallel$, magnetic-field strength $\|\mathbf{B}\|$, Parker spiral angle ϕ_p, clock angle ϕ_c, and Alfvén Mach number M_A between our database (black) and the entire mission (gray). Vertical lines indicate each distribution's median.

shifted towards more tangential IMFs than the nominal Parker spiral angles of $\sim 35°$–$40°$ at Venus (Luhmann, 1986; Luhmann et al., 1993).

3 Methodology

3.1 Venus Sun Electric Field (VSE) Frame

Since the plasma environments of unmagnetized bodies are more susceptible to upstream conditions due to the close interaction of the solar wind with the bodies' atmospheres (Bertucci et al., 2011; Brain et al., 2016; Futaana et al., 2017), we will use a reference frame defined by the solar-wind velocity, the IMF, and the convective electric field. We first address how to correct for the solar-wind aberration. Commonly, studies invoke a typical yet constant value from existing literature for the aberration angle (see, for example, Russell et al. (1988), Martinecz et al. (2008), Zhang et al. (2010), or Chai et al. (2015)). To investigate the applicability of such assumption at Venus we display in Figure 3 our database's solar-wind aberration angles. The median of 5.2° agrees well with the nominal value of 5° arising from orbital motion; 61% of the orbits have aberrations less than 10° from this value. Still, a significant number of orbits have larger aberrations, so we will rotate the scans' positions about the $+Z_{VSO}$ axis to correct for each orbit's median solar-wind aberration. This transforms into an aberrated VSO frame in which each orbit's median solar-wind velocity $\mathbf{v}_{SW}$ points along the $-X_{VSO}$ axis.

We next transform from this aberrated VSO frame into the Venus-Sun-Electric field (VSE) frame. The X_{VSE} axis is the same as the aberrated X_{VSO} axis. We define $+Y_{VSE}$ as the direction of the cross-flow component of the upstream IMF, making $+Z_{VSE}$ point along the upstream convective electric field $\mathbf{E} = -\mathbf{v}_{SW} \times \mathbf{B}_{IMF}$. We refer to the hemispheres in the $\pm Y_{VSE}$ directions as the $\pm B$ hemispheres and in the $\pm Z_{VSE}$ directions as the $\pm E$ hemispheres. Transforming into this frame entails rotating the aberrated VSO frame about the X_{VSO} axis clockwise by the median upstream IMF clock angle. We show in Figure 4 the resulting locations of the magnetosheath scans in VSE latitude-longitude space (defined analogously as in VSO). The measurements are better distributed in this frame except for a 'subsolar-wind hole'; VEX's orbits, chosen to explore the near-wake region of the magnetotail ($X_{VSE} \lesssim -1.5\ R_V$) (Futaana et al., 2017), lead to the undersampling of this region. We include the same example orbits to illustrate how the transformation affects scan positions.

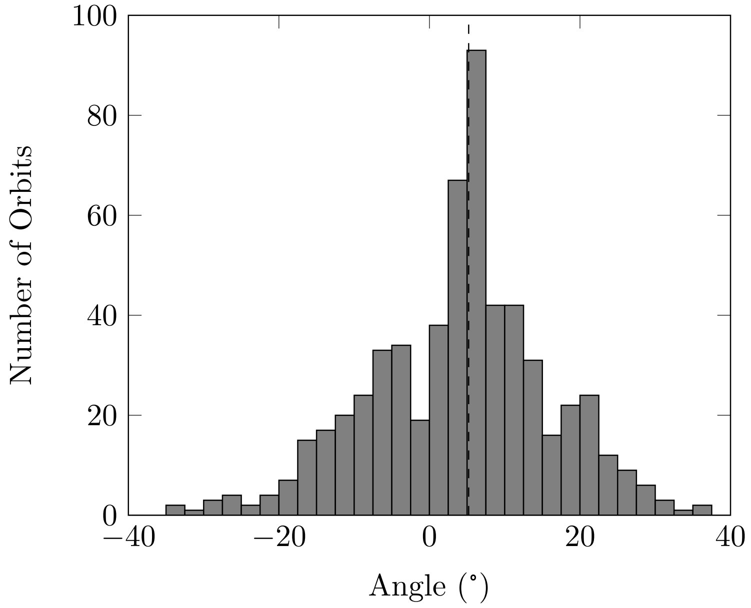

Figure 3. Distribution of the solar-wind aberration angles for our database's orbits. The dashed line indicates the median value of 5.2° which agrees with the nominal value of 5°.

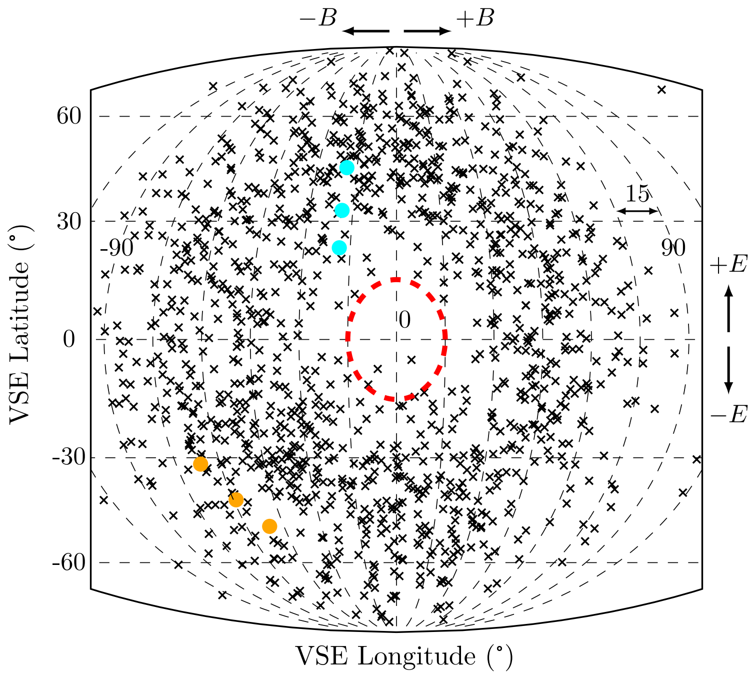

Figure 4. Location of the magnetosheath scans in the VSE latitude-longitude frame. The red circle with radius 15° indicates the 'subsolar-wind hole' of data coverage. The aqua and orange markers highlight the same scans as in Figure 1

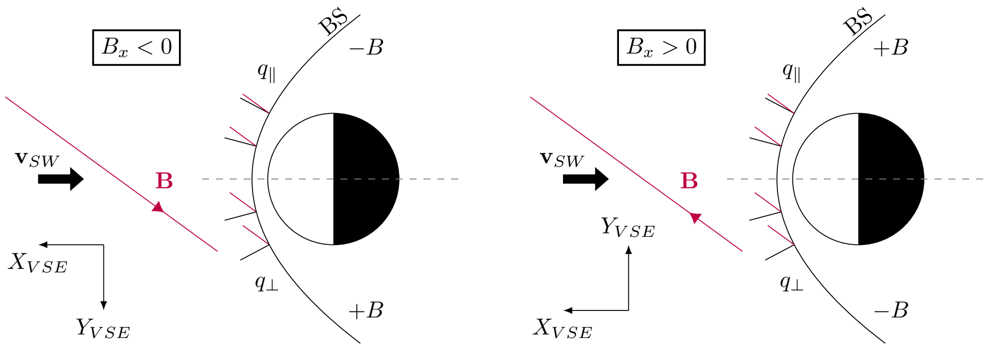

Figure 5. The sign of B_x in the VSE frame determines in which B hemisphere the $q_{\perp}$ and $q_{\|}$ portions of the bow shock lie. Note that for substantially tangential ($B_x \approx 0$) or radial ($B_y \approx 0$) IMFs the difference in bow-shock geometry between the $\pm B$ hemispheres is small. The example $\mathbf{B}$ has the nominal Parker spiral angle of 36° (Slavin & Holzer, 1981).

3.2 $q_{\perp}$ and $q_{\|}$ Hemispheres

Once in the VSE frame, we sort the measurements' locations based on the bow-shock geometry. As Figure 5 illustrates, the $q_{\perp}$ and $q_{\|}$ sections of the bow shock and magnetosheath can lie in either B hemisphere depending on whether the IMF spiral is outwards ($B_x < 0$) or inwards ($B_x > 0$). Comparing plasma parameters between $q_{\perp,\|}$ hemispheres is more suitable since many magnetosheath characteristics and processes depend on the bow-shock geometry, not the direction of the magnetic field relative to Venus (see e.g., Luhmann et al. (1987), Xiao et al. (2018), or Jarvinen et al. (2020)). Thus, to transform from $\pm B$ to $q_{\perp,\|}$, we reflect when needed the location of the measurements about the XZ–plane, i.e. flip the sign of their VSE longitude. Similar amounts of scans flip between hemispheres, so the transformation negligibly changes the spatial coverage shown in Figure 4. This places 663 measurements in the $q_{\perp}$ hemisphere and 518 in the $q_{\|}$ one.

3.3 Longitudinal Binning

Previous works characterize plasma asymmetries through spatial maps of average parameters and/or by comparing the parameters' bulk statistics and ratios between hemispheres (Paularena et al., 2001; Longmore et al., 2005; Chaston et al., 2013; Dimmock & Nykyri, 2013; Du et al., 2013; Xiao et al., 2018). Since we are interested in asymmetries between the $q_{\perp,\parallel}$ hemispheres, we average over both latitude (i.e. $\pm E$ hemispheres) and radial distance from the planet. We thus follow a similar method as B. M. Walsh et al. (2012) and sort our measurements into 15°-wide longitudinal bins. Our bins however have a 50% overlap so as to present a running average of the parameters.

3.4 Distribution of Ratios

Properly calculating the ratio of parameters between two hemispheres while accounting for solar-wind conditions is not necessarily straightforward. Many Earth studies (see Section 1) have the advantage that spacecraft sampled both hemispheres (e.g dawn and dusk) during the same orbit. No bias with respect to upstream conditions then exists between hemispheres and measurements can be paired up to calculate distributions of parameter ratios. In contrast, VEX's quasi-polar orbit generally lead to narrow longitudinal sampling (regardless of frame), so measurement-by-measurement pairing is not possible. An alternative is to merely take the ratio of parameter medians between corresponding longitudinal bins or hemispheres as a whole. The ratio of the medians is however an inferior statistical product since it has more uncertainty and worse reproducibility than the median of the ratios (Brody et al., 2002). Additionally, this tactic does not produce a distribution whose spread provides a sense of the ratio's variability. Ratio distributions are heavy-tailed and may not have definable moments (Brody et al., 2002) (e.g. the ratio distribution of two normally distributed random variables is Lorentzian (Geary, 1930; Fieller, 1932)), so deriving a measure of spread is important for interpreting the results. To address this challenge, we take an approach which involves the inverse transform sampling of estimates of the measurements' cumulative distribution functions (CDFs). Our method is similar to Possolo et al. (2019)'s, with the difference that we have access to the measurement distributions and use a non-parametric method for estimating CDFs.

Consider the distributions of the normalized parameter $\widehat{a}$ in two bins centered at corresponding longitudes in the $q_\perp$ and $q_\parallel$ hemispheres. We wish to calculate enough values of the ratio $\overline{a} = \widehat{a}_{q_\perp}/\widehat{a}_{q_\parallel}$ to construct a representative distribution of the parameter asymmetry. Since the number of measurements in each bin is not that high (20–150), by directly sampling the measurements we can only generate $\mathcal{O}(10^2{-}10^4)$ distinct values of the ratio. If we drew $\mathcal{O}(10^6)$ samples from each bin (a typical size in random sampling techniques (Possolo et al., 2019)), the resulting ratio distribution may be overly discretized due to the few measurements and the assumption that they are error-free.

Therefore, to smooth $\overline{a}$ and introduce some measurement uncertainty, we approximate the CDF of $\widehat{a}$ in each bin using Gaussian kernel density estimates (KDEs) (Sheather, 2004) with a resolution of $\mathcal{O}(10^5)$ points. We then draw a 10^6 random values of $\widehat{a}$ from each bin's CDF and compute the corresponding $\overline{a}$ to generate our ratio distribution for that longitudinal position. Appendix A provides more detail for this procedure.

The advantage of KDEs is that we avoid having to justify which particular model best fits the measurement distributions and how we optimize its free parameters (cf. Possolo et al. (2019)). The only free parameter with KDEs is a smoothing parameter k called the bandwidth which is related to the uncertainty of the measurement (higher bandwidth means higher uncertainty). We find that choosing $k \in [0.01, 0.1]$ provides adequate smoothing while maintaining agreement between the quartiles and histograms of the random samples and the measurements. Higher values oversmooth and spread out the distributions. The choice of k within that range negligibly affects the medians and quartiles presented next.

4 Results

We show in Figure 6 the medians of the magnetosheath measurements (left column) and of their normalized values (right column) as a function of longitude along the $q_{\perp/\parallel}$ hemispheres. Bins less than 70° (50°) from the central meridian contain more than 60 (100) scans each. We depict the first and third quartiles as 'error' bars but these reflect the distributions' spread, not uncertainties in the medians. This depiction is meant to visualize how the measurement distributions shift from bin to bin.

Overall the data follows the expected trend of higher plasma deceleration, compression, and heating closer to the central meridian (Spreiter & Alksne, 1966; Spreiter et al., 1970; B. M. Walsh et al., 2012; Dimmock & Nykyri, 2013; Jarvinen et al., 2013). The slight increase of plasma speed near 0° is likely an artifact of the poor data coverage near the subsolar region; the normalized magnetic field strength shows a slight analogous dip though the normalized temperatures do not. These bins mostly contain measurements at latitudinal distances greater than 30° (see Figure 4), so measurements of the parameters at the 'nose' of the obstacle are underrepresented.

In Figure 7 we plot the medians of the parameter asymmetries as a function of longitudinal distance from the central meridian. Again the 'error' bars indicate the first and third quartiles as a measure of the distributions' spread, not uncertainty. We also present in Figure 8 the same quartiles but for ratios of the measurements across all longitudes in each hemisphere. These results are not calculated from those in Figure 7, but rather we rerun the procedure from Section 3.4 using only one bin spanning 0–90° per hemi-

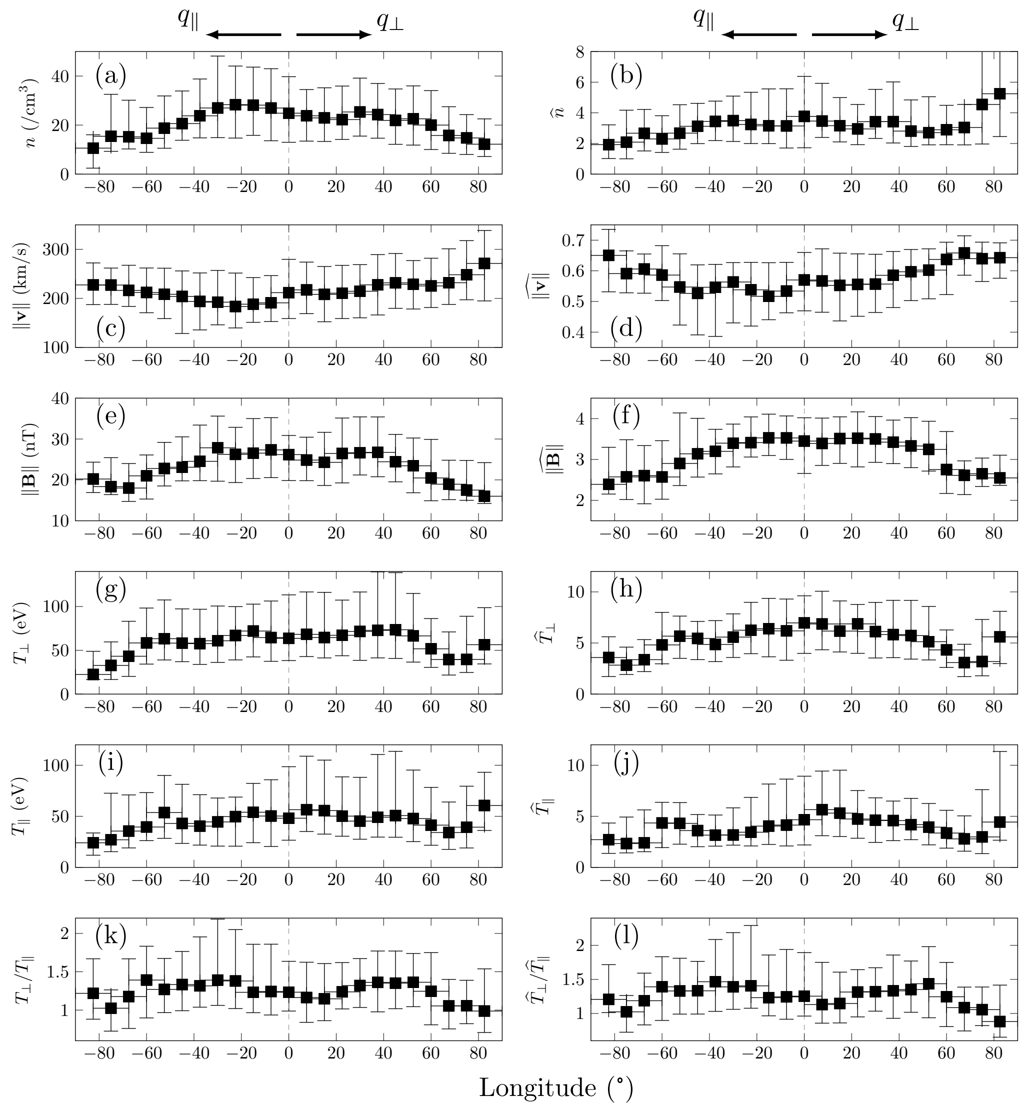

Figure 6. Proton parameters as a function of longitudinal distance from the central meridian. The left column shows unnormalized values, the right column normalized. Positive longitude corresponds to the $q_\perp$ hemisphere, negative to the $q_\parallel$ hemisphere. Markers indicate medians while 'error' bars correspond to the first and third quartiles.

sphere. We also show the results for the data subsets corresponding to high (> 7.5) and low (< 5.5) solar-wind Alfvén Mach numbers (the median for all data is 6.5).

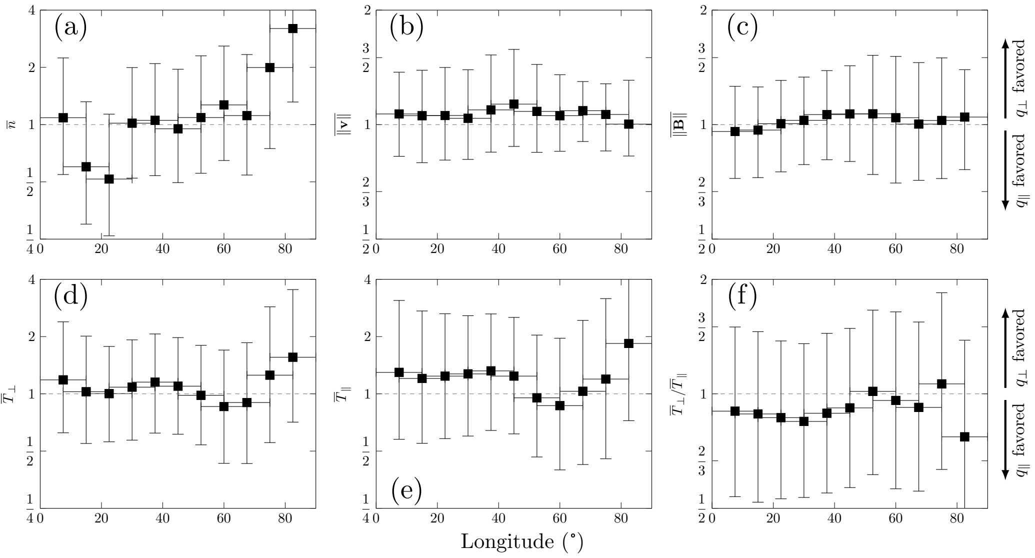

Figure 7. Proton parameter asymmetries as a function of longitudinal distance from the central meridian. The asymmetry favors the $q_\perp$ hemisphere if $\overline{a} > 1$ and the $q_\parallel$ hemisphere if $\overline{a} < 1$. Markers indicate medians while 'error' bars correspond to the first and third quartiles. Note the varying vertical scales.

4.1 Plasma Density and Speed

On average we find ∼18% higher densities in the $q_\parallel$ hemisphere across all longitudes, however this value varies considerably as a function of longitude (see Figure 7a), which creates the large spread in $\overline{n}$. In contrast, $\overline{\|\mathbf{v}\|}$ has much narrower distributions which indicate ∼7% lower average speeds in the $q_\parallel$ hemisphere. These asymmetries mirror those measured between Earth's dawn and dusk hemispheres as well as follow the same trend with M_A (Longmore et al., 2005; B. M. Walsh et al., 2012). Even though these studies do not use reference frames analogous to VSE or with $q_{\perp/\parallel}$ hemispheres, the average Parker spiral angle at Earth (∼45°) (Slavin & Holzer, 1981) makes it so that, statistically, dawn corresponds to $q_\parallel$ and dusk to $q_\perp$. Dimmock and Nykyri (2013) did use $q_{\perp/\parallel}$ hemispheres and also qualitatively found lower plasma speeds in the $q_\parallel$ hemisphere. They did not detect a density asymmetry, yet attribute this discrepancy to the asymmetry's "magnitude [not being] distinguishable on [their] color scale."

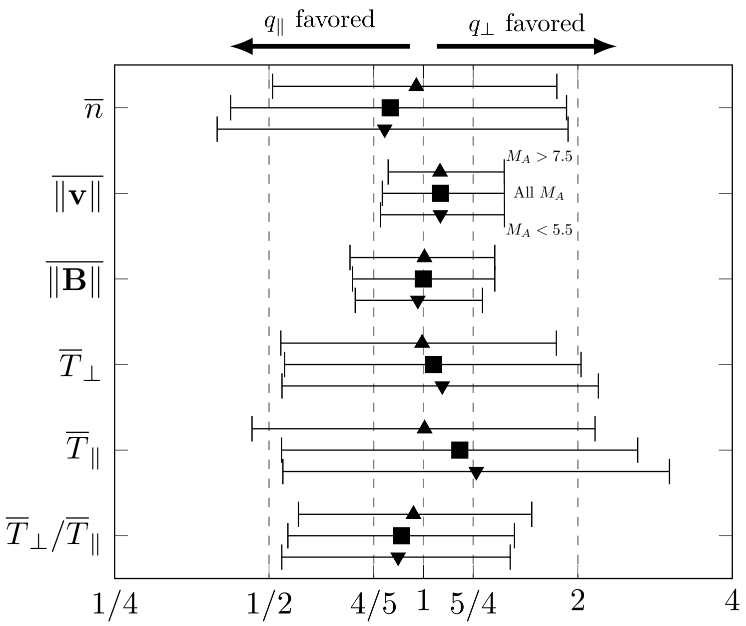

Figure 8. Proton parameter asymmetries between the $q_{\perp}$ and $q_{\parallel}$ hemispheres as a function of Alfvén Mach number. For each parameter, the top marker is for $M_A > 7.5$, the middle for all M_A, and the bottom for $M_A < 5.5$. The asymmetry favors the $q_{\perp}$ hemisphere for values greater than 1 and the $q_{\parallel}$ hemisphere for values less than 1. Markers indicate medians while 'error' bars correspond to the first and third quartiles.

At Earth, the nonuniform thickness of the magnetosheath may cause the density asymmetry (B. M. Walsh et al., 2012). The bow shock is a standing fast mode wave which travels faster perpendicular to $\mathbf{B}$ than parallel to it. This means the $q_\perp$ side lies further from the planet than the $q_\parallel$ side, leading to a thicker $q_\perp$ magnetosheath where the plasma is less compressed as it deflects around the obstacle. Venus' bow shock is also closer to the planet on the $q_\parallel$ side than on the $q_\perp$ side (at least at the terminator) (Zhang, Schwingenschuh, et al., 1991), so likely the same reasoning applies. In contrast, there is no explanation for the speed asymmetry at Earth; MHD theory predicts a symmetric profile so potentially considering kinetic effects is required (Dimmock & Nykyri, 2013). At Venus, however, asymmetries in the magnetic-field draping may be involved (see discussion in Section 4.2).

4.2 Magnetic Field Strength

We calculate that med($\overline{\|\mathbf{B}\|}$) $=$ 1 on average so there is no significant asymmetry in the magnetic-field strength despite a slight local $q_\perp$-favored asymmetry at 30–60° longitude (see Figure 7c). This is unexpected given that observations at Earth in dawn-dusk (B. M. Walsh et al., 2012) and $q_{\perp/\parallel}$ (Dimmock & Nykyri, 2013) reference frames as well hybrid simulations of Venus (Jarvinen et al., 2013, 2016) show stronger magnetic fields in the dusk/$q_\perp$ hemisphere. We find that the normalized magnetic-field-strength $\widehat{\|\mathbf{B}\|}$ increases with increasing M_A in both hemispheres, yet $\overline{\|\mathbf{B}\|}$ does not display a clear trend, unlike what is seen in global MHD simulations at Earth (B. M. Walsh et al., 2012). Comparison to other asymmetry studies involving VEX MAG data is limited since none sort measurements into $q_{\perp/\parallel}$ hemispheres for the dayside magnetosheath. However, if we instead keep the data sorted in $\pm B$ hemispheres, we find an overall $\sim$12% stronger field in the $+B$ hemisphere with the highest asymmetries at 50–75° longitude. Figure 2ac in Du et al. (2013) and Figure 7 in Xiao et al. (2018) show a qualitatively similar trend, indicating that we do not have a hidden sampling bias.

Our averaging over latitude and radial distance from the planet likely smears $q_{\perp/\parallel}$ asymmetries discernible in a higher-resolution MAG-only study (e.g., Du et al. (2013), Delva et al. (2017), or Xiao and Zhang (2018)). Additionally, the magnetic-field draping at Venus exhibits solar-cycle dependencies (Zhang, Luhmann, & Russell, 1991; Xiao & Zhang, 2018), so further characterization throughout solar cycle could uncover asymmetries over which we averaged. We only consider $\|\mathbf{B}\|$ yet simulations (Jarvinen et al.,

2013) and observations (Delva et al., 2017) indicate that **B** kinks due to a reversal of B_x only in the $q_\parallel$ magnetosheath. This deformation of **B** may cause the speed asymmetry as the more complex magnetic-field topology hinders the plasma flow more compared to the flow-aligned **B** configuration on the $q_\perp$ side.

4.3 Plasma Temperatures and Temperature Anisotropy

The perpendicular and parallel temperatures are higher in the $q_\perp$ hemisphere by $\sim$5% and $\sim$17%, respectively. The opposite trend occurs at Earth, where temperatures are higher in the dawn/$q_\parallel$ side (B. M. Walsh et al., 2012; Chaston et al., 2013; Dimmock, Nykyri, et al., 2015). We also find that the temperature anisotropy is higher in the $q_\parallel$ hemisphere by $\sim$10%, again showing the opposite trend to that observed at Earth (Chaston et al., 2013; Dimmock, Osmane, et al., 2015; Soucek et al., 2015). However, at both planets the asymmetries' magnitudes decrease with increasing M_A. To delve into these results further, we detail in Table 1 the dependence on M_A of the medians of the normalized parameters in each hemisphere. Both temperatures appear insensitive to M_A in the $q_\perp$ hemisphere, leading to a fairly constant temperature anisotropy. In contrast, in the $q_\parallel$ hemisphere the medians of $\widehat{T}_\perp$ and $\widehat{T}_\parallel$ increase by 20% and 37%, respectively, between low and high Mach numbers. The unnormalized parameters follow nearly identical quantitative trends since for all M_A in both hemispheres we find that $\text{med}(T_{\perp,SW}) = \text{med}(T_{\parallel,SW}) \approx$ 11 eV. This suggests that our results do not arise from an unexpected sampling bias but rather from differences in relevant heating or thermalization processes at Venus and Earth's magnetosheaths.

Table 1. Medians of Normalized Temperatures and Temperature Anisotropy

	$q_\parallel$			$q_\perp$		
M_A:	Low	All	High	Low	All	High
$\text{med}(\widehat{T}_\perp)$:	4.6	5.3	5.5	5.4	5.6	5.6
$\text{med}(\widehat{T}_\parallel)$:	3.0	3.4	4.1	4.2	4.3	4.1
$\text{med}(\widehat{T}_\perp/\widehat{T}_\parallel)$:	1.44	1.36	1.31	1.28	1.25	1.27

5 Discussion

5.1 Dependence on IMF Orientation

The physical mechanisms creating and sustaining the asymmetries observed in planetary magnetosheaths are the subject of ongoing research. At Earth, the upstream IMF's orientation and its role in processes captured by MHD models provide partial insight into the physics (Němeček et al., 2002; Longmore et al., 2005; B. M. Walsh et al., 2012; Dimmock & Nykyri, 2013; Dimmock, Nykyri, et al., 2015; Haaland et al., 2017). However, persisting discrepancies with MHD and hybrid simulations suggest IMF orientation may not even be a controlling factor at all (B. M. Walsh et al., 2012; Dimmock, Nykyri, et al., 2015; Turc et al., 2020). Thus, boundary phenomena at the magnetopause (e.g. subsolar magnetic reconnection or flux transfer events) and/or kinetic phenomena in the magnetosheath (e.g. instabilities and turbulence) must also be involved (Dimmock, Nykyri, et al. (2015), Dimmock et al. (2017), and references therein).

To check whether this is the case at Venus as well, we first explore the asymmetries' dependence on IMF orientation by taking advantage of the reduced configuration space provided by the $q_{\perp,\parallel}$ frame. This frame constrains the IMF to only make 0–90° angles with respect to the $-X_{VSE}$ axis, always in the direction of the $q_\perp$ hemisphere. This enables simple comparison with simulations as these also only consider such small range of IMF orientations. For example, Jarvinen et al. (2013) qualitatively find a $q_\perp$-favored magnetic-field-strength asymmetry in Venus' dayside magnetosheath when the upstream IMF has an angle of 36° with respect to the solar-wind velocity; when the IMF is perpendicular to the solar-wind velocity, the asymmetry disappears. The authors do not discuss asymmetries in plasma density or speed, though none are apparent in the spatial maps presented.

To compare with these results, we select the scans with corresponding IMF angles between 80–90° (near tangential, 192 scans) and between 26–46° (near Parker spiral, 287 scans). We recalculate the overall $q_{\perp,\parallel}$ asymmetries for these subsets and find that $\widehat{\|\mathbf{v}\|}$, $\widehat{\|\mathbf{B}\|}$, $\widehat{T}_\perp$, and $\widehat{T}_\perp/\widehat{T}_\parallel$ exhibit slightly lower levels of asymmetry for near-tangential IMFs than for near-Parker-spiral IMFs, in line with the trends in Jarvinen et al. (2013). On the other hand, $\widehat{n}$ and $\widehat{T}_\parallel$ exhibit median asymmetries of $\sim$10% and $\sim$25%, respectively, for near-tangential IMFs, yet only $\sim$5% asymmetries for near-Parker-spiral IMFs. As this is contrary to the expectations from MHD theory and simulations, the IMF orientation by itself cannot explain the asymmetries at Venus either.

5.2 Connection with Turbulence and Instabilities

The findings above along with the fact that magnetopause boundary phenomena are less significant at Venus imply that differences in kinetic phenomena between the $q_\perp$ and $q_\parallel$ magnetosheaths affect the plasma asymmetries. Investigating this relationship is especially important given that $\overline{T}_\perp$, $\overline{T}_\parallel$, and $\overline{T}_\perp/\overline{T}_\parallel$ follow trends at Venus which oppose those at Earth. Such a dedicated study is beyond the scope of this paper, so we instead briefly discuss some relevant kinetic processes present in planetary magnetosheaths to provide tentative directions for continued research.

Several studies indicate that $q_\parallel$ magnetosheaths exhibit stronger turbulent fluctuations than $q_\perp$ magnetosheaths (see Lucek et al. (2005), Dimmock et al. (2017), and references therein). Additionally, various ion-scale high-frequency phenomena dominate the $q_\parallel$-magnetosheath turbulence, whereas low-frequency temperature-anisotropy instabilities dominate in the $q_\perp$ magnetosheath (Dimmock et al., 2017). These differences possibly lead to higher non-adiabatic heating of ions in the $q_\parallel$ magnetosheath, which could explain the $q_\parallel$-favored temperature asymmetries observed at Earth (Chaston et al., 2013; Dimmock et al., 2017). Venus' magnetosheath does exhibit inertial-scale and kinetic-scale turbulence (Vörös et al., 2008; Bowen et al., 2021), with fully developed turbulence more likely in the $q_\parallel$ magnetosheath (Xiao & Zhang, 2018). A variety of plasma waves (Strangeway, 1991; Du et al., 2010; Futaana et al., 2017; Fränz et al., 2017) can act as sources for this turbulence, many of which are also present in Earth's magnetosheath (Lacombe & Belmont, 1995; Schwartz et al., 1996). Yet, since Venus' magnetosheath is smaller than Earth's ($\lesssim$ 6000 km thick compared to $\gtrsim$ 18,000 km thick (Russell et al., 1988; Farris et al., 1991; Whittaker et al., 2010; B. M. Walsh et al., 2012)), the turbulent processes in the $q_\parallel$ magnetosheath may be unable to impact global particle properties before the plasma flows past.

Also important are electromagnetic ion-cyclotron (EMIC) waves and mirror modes (MMs), both of which limit the extent of turbulent heating so as to maintain magnetosheaths marginally stable by redistributing energy from $T_\perp$ to $T_\parallel$ (Fuselier et al., 1994; Soucek et al., 2008; Chaston et al., 2013; Dimmock, Osmane, et al., 2015). The temperature anisotropy

$T_\perp/T_\parallel$ as well as the perpendicular and parallel plasma betas

$$\beta_{\perp,\parallel} = \frac{nT_{\perp,\parallel}}{\|\mathbf{B}\|^2/2\mu_0} \tag{1}$$

control the growth rates, instability criteria, and other important characteristics of these instabilities (Gary, 1992; Gary et al., 1993). We already found in Section 4.3 a $q_\parallel$-favored asymmetry for $T_\perp/T_\parallel$; similar analysis reveals $q_\perp$-favored asymmetries for both $\beta_\perp$ (∼15%) and $\beta_\parallel$ (∼26%). Consequently, $T_\perp/T_\parallel$ is higher when $\beta_\parallel$ is lower and vice versa, which is an inverse correlation characteristic of the instability threshold for EMIC waves (Gary et al., 1976). These waves drive plasma to marginal stability by reducing the temperature anisotropy through pitch-angle scattering (Gary et al., 1993; Fuselier et al., 1994). Possibly then the same wave-particle interactions are occurring in both magnetosheath geometries at Venus. As for MMs, the linear instability criterion requires that

$$1 + \beta_\perp \left(1 - \frac{T_\perp}{T_\parallel}\right) < 0 \tag{2}$$

for the mode to develop (Hasegawa, 1969). While we do find that $T_\perp/T_\parallel > 1$ in both hemispheres of the magnetosheath (see Figure 6k), the opposing $T_\perp/T_\parallel$ and $\beta_\perp$ asymmetries complicates assessing the asymmetries' expected impact on MM activity. Additionally, MMs are not uniformly distributed across the magnetosheath (Volwerk et al., 2016; Fränz et al., 2017), so our averaging over the radial coordinate may obscure important details. These initial results however encourage further investigations of the interplay between plasma parameter asymmetries and turbulent heating/thermalization in planetary magnetosheaths.

6 Conclusions

In this paper we characterized the asymmetries between Venus' $q_\perp$ and $q_\parallel$ magnetosheaths of proton bulk parameters measured by Venus Express' ion mass-energy spectrometer. The main results are as follows:

1. The density exhibits a $q_\parallel$-favored asymmetry analogous to the one at Earth caused by the asymmetry in magnetosheath thickness.
2. The bulk speed exhibits a $q_\perp$-favored asymmetry which is possibly connected to the kinking of $\mathbf{B}$ in the $q_\parallel$ magnetosheath.

3. The magnetic field strength shows no significant asymmetry, though this may result from our measurements' coarse spatial resolution.
4. The perpendicular and parallel temperatures have $q_\perp$-favored asymmetries and the temperature anisotropy has a $q_\parallel$-favored asymmetry. These trends oppose those at Earth and indicate that the different spatial scales of the two magnetosheaths, which lead to different plasma residence times, may affect how much turbulent heating and thermalization processes manage to affect global particle properties.

The last point provides an interesting opportunity for combining comparative planetology and plasma turbulence studies to better understand magnetosheath physics. Investigations comparing particle and electromagnetic-field data taken at magnetized and unmagnetized planets (especially Earth and Venus given their many similarities) can provide new insight into the global impact of kinetic processes in magnetospheric plasmas.

Appendix A Constructing a Ratio Distribution

In this appendix we illustrate how we generate the distribution of ratios of normalized parameters which we use to quantify asymmetries. Consider for example the measurements of normalized density $\widehat{n} = n/n_{SW}$ contained in the bin centered at 45° longitude in the $q_\perp$ magnetosheath. Figure A1 shows a histogram of these data along with the individual values at the top. To convert the set of discrete values into a continuous PDF we use Gaussian KDEs to 'spread' each measurement over a finite domain, effectively stretching each measurement's delta PDF into a Gaussian PDF. The bandwidth k of the KDEs determines the width of the Gaussian; we use $k \in [0.01, 0.1]$. We then add these Gaussian PDFs and normalize to produce the continuous estimate for the PDF also shown in Figure A1. Note that measurements close to zero 'spread' to non-zero values, however the contribution in this region is negligible (less than 5%) for the bandwidths in the range used, so we truncate at zero when converting the PDF into the CDF shown in Figure A2. We then draw random samples $\{\ldots, x_i, \ldots, x_j, \ldots\}$ from the uniform distribution over $[0, 1]$ to generate samples $\{\ldots, \widehat{n}_i, \ldots, \widehat{n}_j, \ldots\}$ of the normalized density through an inverse transform sampling of the estimated CDF. Finally, we repeat the entire procedure with the measurements contained in the bin centered at 45° longitude in the $q_\parallel$ magnetosheath to produce another set of samples of normalized density. Taking the element-wise ratio $\widehat{n} = \widehat{n}_{q_\perp}/\widehat{n}_{q_\parallel}$ of these sets yields the desired distribution of ratios to quantify the asymmetry.

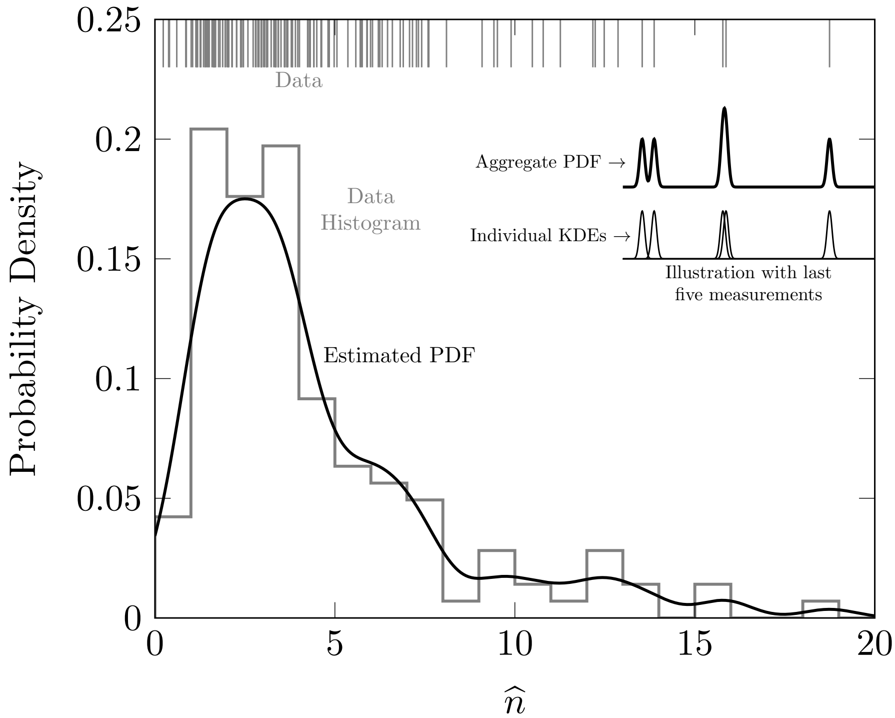

Figure A1. Example of estimating the PDF of discrete measurements using Gaussian KDEs. The curves in the top right illustrate how we sum the KDEs for individual measurements into a single PDF. The data are from the bin centered at 45° longitude in the $q_{\perp}$ magnetosheath.

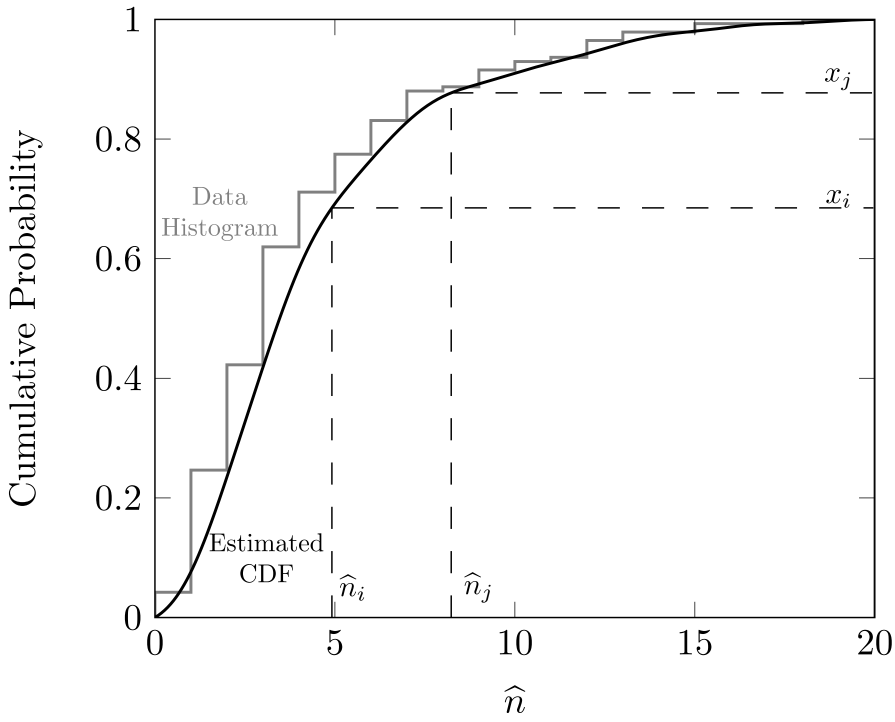

Figure A2. Example of the inverse transform sampling of the CDF estimated using Gaussian KDEs. For each randomly generated x in [0, 1] the CDF assigns a corresponding $\widehat{n}$. The data are from the bin centered at 45° longitude in the $q_\perp$ magnetosheath.

Open Research Section

All VEX data are publicly accessible at the ESA Planetary Science Archive at https://archives.esac.esa.int/psa/ftp/VENUS-EXPRESS/. The dayside magnetosheath data are available in the in-text data citation Rojas Mata and Futaana (2022).

Acknowledgments

SRM was funded by the Swedish National Space Agency under contracts 145/19 and 79/19.

References

Andrews, D. J., Opgenoorth, H. J., Edberg, N. J., André, M., Fränz, M., Dubinin, E., . . . Witasse, O. (2013). Determination of local plasma densities with the MARSIS radar: Asymmetries in the high-altitude Martian ionosphere. *Journal of Geophysical Research: Space Physics*, *118*(10), 6228–6242. doi: 10.1002/jgra.50593

Bader, A., Stenberg Wieser, G., André, M., Wieser, M., Futaana, Y., Persson, M., . . . Zhang, T. (2019). Proton Temperature Anisotropies in the Plasma Environment of Venus. *Journal of Geophysical Research: Space Physics*, *124*(5), 3312–3330. doi: 10.1029/2019JA026619

Barabash, S., Fedorov, A., Sauvaud, J. J., Lundin, R., Russell, C. T., Futaana, Y., . . . Bochsler, P. (2007). The loss of ions from Venus through the plasma wake. *Nature*, *450*(7170), 650–653. doi: 10.1038/nature06434

Barabash, S., Sauvaud, J. A., Gunell, H., Andersson, H., Grigoriev, A., Brinkfeldt, K., . . . Bochsler, P. (2007). The Analyser of Space Plasmas and Energetic Atoms (ASPERA-4) for the Venus Express mission. *Planetary and Space Science*, *55*(12), 1772–1792. doi: 10.1016/j.pss.2007.01.014

Bertucci, C., Duru, F., Edberg, N. J., Fränz, M., Martinecz, C., Szego, K., & Vaisberg, O. (2011). *The induced magnetospheres of mars, venus, and titan* (Vol. 162) (No. 1-4). doi: 10.1007/s11214-011-9845-1

Bowen, T. A., Bale, S. D., Bandyopadhyay, R., Bonnell, J. W., Case, A., Chasapis, A., . . . Whittlesey, P. (2021). Kinetic-Scale Turbulence in the Venusian Magnetosheath. *Geophysical Research Letters*, *48*, 1–12. doi: 10.1029/2020GL090783

Brain, D. A., Bagenal, F., Ma, Y. J., Nilsson, H., & Stenberg Wieser, G. (2016). Atmospheric escape from unmagnetized bodies. *Journal of Geophysical Research: Planets*, *121*(12), 2364–2385. doi: 10.1002/2016JE005162

Brody, J. P., Williams, B. A., Wold, B. J., & Quake, S. R. (2002). Significance and statistical errors in the analysis of DNA microarray data. *Proceedings of the National Academy of Sciences of the United States of America*, *99*(20), 12975–12978. doi: 10.1073/pnas.162468199

Carbary, J. F., Mitchell, D. G., Rymer, A. M., Krupp, N., Hamilton, D., Krimigis, S. M., & Badman, S. V. (2017). Local Time Asymmetries in Saturn's Magnetosphere. In *Dawn-dusk asymmetries in planetary plasma environments* (pp. 323–336). American Geophysical Union (AGU). Retrieved from `https://agupubs.onlinelibrary.wiley.com/doi/abs/10.1002/9781119216346.ch25` doi: https://doi.org/10.1002/9781119216346.ch25

Chai, L., Wan, W., Fraenz, M., Zhang, T., Dubinin, E., Wei, Y., ... Futaana, Y. (2015). Solar zenith angle-dependent asymmetries in Venusian bow shock location revealed by Venus Express. *Journal of Geophysical Research: Space Physics*, *120*(6), 4446–4451. doi: 10.1002/2015JA021221

Chaston, C. C., Yao, Y., Lin, N., Salem, C., & Ueno, G. (2013). Ion heating by broadband electromagnetic waves in the magnetosheath and across the magnetopause. *Journal of Geophysical Research: Space Physics*, *118*, 5579–5591. doi: 10.1002/jgra.50506

Delva, M., Volwerk, M., Jarvinen, R., & Bertucci, C. (2017). Asymmetries in the Magnetosheath Field Draping on Venus' Nightside. *Journal of Geophysical Research: Space Physics*, *122*(10), 10,396–10,407. doi: 10.1002/2017JA024604

Dimmock, A. P., & Nykyri, K. (2013). The statistical mapping of magnetosheath plasma properties based on THEMIS measurements in the magnetosheath interplanetary medium reference frame. *Journal of Geophysical Research: Space Physics*, *118*(8), 4963–4976. doi: 10.1002/jgra.50465

Dimmock, A. P., Nykyri, K., Karimabadi, H., Osmane, A., & Pulkkinen, T. I. (2015). A statistical study into the spatial distribution and dawn-dusk asymmetry of dayside magnetosheath ion temperatures as a function of upstream solar wind conditions. *Journal of Geophysical Research: Space Physics*, *120*, 2767–2782. doi: 10.1002/2014JA020734

Dimmock, A. P., Osmane, A., Pulkkinen, T. I., & Nykyri, K. (2015). A statistical study of the dawn-dusk asymmetry of ion temperature anisotropy and mirror mode occurrence in the terrestrial dayside magnetosheath using THEMIS data. *Journal of Geophysical Research: Space Physics*, *120*(7), 5489–5503. doi: 10.1002/2015JA021192

Dimmock, A. P., Osmane, A., Pulkkinen, T. I., Nykyri, K., & Kilpua, E. (2017). Temperature variations in the dayside magnetosheath and their dependence on ion-scale magnetic structures: THEMIS statistics and measurements by MMS. *Journal of Geophysical Research: Space Physics*, *122*(6), 6165–6184. doi: 10.1002/2016JA023729

Du, J., Wang, C., Zhang, T., & Kallio, E. (2013). Asymmetries of the magnetic field line draping shape around Venus. *Journal of Geophysical Research: Space Physics*, *118*(11), 6915–6920. doi: 10.1002/2013JA019127

Du, J., Zhang, T., Baumjohann, W., Wang, C., Volwerk, M., Vörös, Z., & Guicking, L. (2010). Statistical study of low-frequency magnetic field fluctuations near Venus under the different interplanetary magnetic field orientations. *Journal of Geophysical Research*, *115*(A12251). doi: 10.1029/2010JA015549

Dubinin, E., Chanteur, G., Fraenz, M., Modolo, R., Woch, J., Roussos, E., … Winningham, J. D. (2008). Asymmetry of plasma fluxes at Mars. ASPERA-3 observations and hybrid simulations. *Planetary and Space Science*, *56*(6), 832–835. doi: 10.1016/j.pss.2007.12.006

Dubinin, E., Fraenz, M., Woch, J., Modolo, R., Chanteur, G., Duru, F., … Lundin, R. (2012). Upper ionosphere of Mars is not axially symmetrical. *Earth, Planets and Space*, *64*(2), 113–120. doi: 10.5047/eps.2011.05.022

Farris, M. H., Petrinec, S. M., & Russell, C. T. (1991). The Thickness of the Magnetosheath: Constraints on the Polytropic Index. *Geophysical Research Letters*, *18*(10), 1821–1824.

Fieller, E. C. (1932). The Distribution of the Index in a Normal Bivariate Population. *Biometrika*, *24*(3/4), 428–440. Retrieved from `https://www.jstor.org/stable/2331976`

Fränz, M., Dubinin, E., Roussos, E., Woch, J., Winningham, J. D., Frahm, R. A., … Lundin, R. (2006). Plasma moments in the environment of mars: Mars express ASPERA-3 observations. *Space Science Reviews*, *126*(1-4), 165–207. doi: 10.1007/s11214-006-9115-9

Fränz, M., Echer, E., Marques de Souza, A., Dubinin, E., & Zhang, T. (2017). Ultra low frequency waves at Venus: Observations by the Venus Express spacecraft. *Planetary and Space Science*, *146*(August), 55–65. doi: 10.1016/j.pss.2017.08.011

Fuselier, S. A., Anderson, B. J., Gary, S. P., & Denton, R. E. (1994). Inverse correlations between the ion temperature anisotropy and plasma beta in the Earth's quasi-parallel magnetosheath. *Journal of Geophysical Research*, *99*(A8), 14931. doi: 10.1029/94ja00865

Futaana, Y., Stenberg Wieser, G., Barabash, S., & Luhmann, J. G. (2017). Solar Wind Interaction and Impact on the Venus Atmosphere. *Space Science Reviews*, *212*(3-4), 1453–1509. Retrieved from `http://dx.doi.org/10.1007/s11214-017-0362-8` doi: 10.1007/s11214-017-0362-8

Gary, S. P. (1992). The Mirror and Ion Cyclotron Anisotropy Instabilities. *Journal of Geophysical Research*, *97*(A6), 8519–8529.

Gary, S. P., Fuselier, S. A., & Anderson, B. J. (1993). Ion anisotropy instabilities in the magnetosheath. *Journal of Geophysical Research: Space Physics*, *98*(A2), 1481–1488. doi: 10.1029/92ja01844

Gary, S. P., Montgomery, M. D., Feldman, W. C., & Forslund, D. W. (1976). Proton Temperature Anisotropy Instabilities in the Solar Wind. *Journal of Geophysical Research*, *81*(7), 1241–1246.

Geary, R. C. (1930). The Frequency Distribution of the Quotient of Two Normal Variates. *Journal of the Royal Statistical Society*, *93*(3), 442–446. Retrieved from `https://www.jstor.org/stable/2342070`

Gupta, N., Venkateswara Rao, N., & Kadhane, U. R. (2019). Dawn-Dusk Asymmetries in the Martian Upper Atmosphere. *Journal of Geophysical Research: Planets*, *124*(12), 3219–3230. doi: 10.1029/2019JE006151

Haaland, S., Runov, A., & Forsyth, C. (Eds.). (2017). *Dawn-Dusk Asymmetries in Planetary Plasma Environments.* American Geophysical Union (AGU). Retrieved from `https://agupubs.onlinelibrary.wiley.com/doi/book/10.1002/9781119216346` doi: 10.1002/9781119216346

Halekas, J. S., Brain, D. A., Luhmann, J. G., DiBraccio, G. A., Ruhunusiri, S., Harada, Y., ... Jakosky, B. M. (2017). Flows, Fields, and Forces in the Mars-Solar Wind Interaction. *Journal of Geophysical Research: Space Physics*, *122*(11), 11,320–11,341. doi: 10.1002/2017JA024772

Hasegawa, A. (1969). Drift mirror instability in the magnetosphere. *Physics of Fluids*, *12*(12), 2642–2650. doi: 10.1063/1.1692407

Jarvinen, R., Alho, M., Kallio, E., & Pulkkinen, T. I. (2020). Oxygen Ion Escape From Venus Is Modulated by Ultra-Low Frequency Waves. *Geophysical Research Letters*, *47*(11). doi: 10.1029/2020GL087462

Jarvinen, R., Brain, D. A., & Luhmann, J. G. (2016). Dynamics of planetary ions in the induced magnetospheres of Venus and Mars. *Planetary and Space Science*, *127*, 1–14. Retrieved from `http://dx.doi.org/10.1016/j.pss.2015.08.012` doi: 10.1016/j.pss.2015.08.012

Jarvinen, R., Kallio, E., & Dyadechkin, S. (2013). Hemispheric asymmetries of the Venus plasma environment. *Journal of Geophysical Research: Space Physics*, *118*(7), 4551–4563. doi: 10.1002/jgra.50387

Jin, T., Lei, L., Yiteng, Z., Lianghai, X., & Fuhao, Q. (2022). Statistical Analysis of the Distribution and Evolution of Mirror Structures in the Martian Magnetosheath. *The Astrophysical Journal*, *929*(2), 165. Retrieved from `http://dx.doi.org/10.3847/1538-4357/ac5f00` doi: 10.3847/1538-4357/ac5f00

Kallio, E., Chaufray, J. Y., Modolo, R., Snowden, D., & Winglee, R. (2011). Modeling of venus, mars, and titan. *Space Science Reviews*, *162*(1-4), 267–307. doi: 10.1007/s11214-011-9814-8

Kallio, E., Koskinen, H. E., Barabash, S., Lundin, R., Norberg, O., & Luhmann, J. G. (1994). Proton flow in the Martian magnetosheath. *Journal of Geophysical Research*, *99*(A12), 23,547–23,559.

Karimabadi, H., Roytershteyn, V., Vu, H. X., Omelchenko, Y. A., Scudder, J., Daughton, W., . . . Geveci, B. (2014). The link between shocks, turbulence, and magnetic reconnection in collisionless plasmas. *Physics of Plasmas*, *21*(6). doi: 10.1063/1.4882875

Lacombe, C., & Belmont, G. (1995). Waves in the Earth's magnetosheath: Observations and interpretations. *Advances in Space Research*, *15*(8-9), 329–340. doi: 10.1016/0273-1177(94)00113-F

Lapenta, G., Pierrard, V., Keppens, R., Markidis, S., Poedts, S., Šebek, O., . . . Borremans, K. (2013). SWIFF: Space weather integrated forecasting framework. *Journal of Space Weather and Space Climate*, *3*. doi: 10.1051/swsc/2013027

Limaye, S. S., Lebonnois, S., Mahieux, A., Pätzold, M., Bougher, S., Bruinsma, S., . . . Zasova, L. (2017). The thermal structure of the Venus atmosphere: Intercomparison of Venus Express and ground based observations of vertical temperature and density profiles. *Icarus*, *294*, 124–155. doi: 10.1016/j.icarus.2017.04.020

Longmore, M., Schwartz, S. J., Geach, J., Cooling, B. M., Dandouras, I., Lucek, E. A., & Fazakerley, A. N. (2005). Dawn-dusk asymmetries and sub-Alfvénic flow in the high and low latitude magnetosheath. *Annales Geophysicae*, *23*(10), 3351–3364. doi: 10.5194/angeo-23-3351-2005

Lucek, E. A., Constantinescu, D., Goldstein, M. L., Pickett, J., Pinçon, J. L., Sahraoui, F., . . . Walker, S. N. (2005). The magnetosheath. *Space Science Reviews*, *118*, 95–152. doi: 10.1007/s11214-005-3825-2

Luhmann, J. G. (1986). The Solar Wind Interaction with Venus. *Space Science Reviews*, *44*, 241–306.

Luhmann, J. G. (1995). The inner magnetosheath of Venus: An analogue for Earth? *Journal of Geophysical Research*, *100*(A7), 12,035–13,045.

Luhmann, J. G., Russell, C. T., Phillips, J. L., & Barnes, A. (1987). On the role of the quasi-parallel bow shock in ion pickup: A lesson from Venus? *Journal of Geophysical Research*, *92*(A3), 2544–2550. doi: 10.1029/ja092ia03p02544

Luhmann, J. G., Zhang, T., Petrinec, S. M., & Russell, C. T. (1993). Solar Cycle 21 Effects on the Interplanetary Magnetic Field and Related Parameters at 0.7 and 1.0 AU. *Journal of Geophysical Research*, *98*(A4), 5559–5572.

Martinecz, C., Fränz, M., Woch, J., Krupp, N., Roussos, E., Dubinin, E., . . . Lammer, H. (2008). Location of the bow shock and ion composition boundaries at Venus—initial determinations from Venus Express ASPERA-4. *Planetary and Space Science*, *56*(6), 780–784. Retrieved from `https://www.sciencedirect.com/science/article/pii/S0032063307003765` doi: https://doi.org/10.1016/j.pss.2007.07.007

Masunaga, K., Futaana, Y., Yamauchi, M., Barabash, S., Zhang, T. L., Fedorov, A. O., . . . Okano, S. (2011). O+ outflow channels around Venus controlled by directions of the interplanetary magnetic field: Observations of high energy O+ ions around the terminator. *Journal of Geophysical Research: Space Physics*, *116*(9), 1–9. doi: 10.1029/2011JA016705

Modolo, R., Hess, S., Génot, V., Leclercq, L., Leblanc, F., Chaufray, J. Y., ... Holmström, M. (2018). The LatHyS database for planetary plasma environment investigations: Overview and a case study of data/model comparisons. *Planetary and Space Science*, *150*, 13–21. doi: 10.1016/j.pss.2017.02.015

Müller-Wodarg, I. C., Forbes, J. M., & Keating, G. M. (2006). The thermosphere of Venus and its exploration by a Venus Express Accelerometer Experiment. *Planetary and Space Science*, *54*(13-14), 1415–1424. doi: 10.1016/j.pss.2006.04.029

Němeček, Z., Šafránková, J., Zastenker, G. N., Pišoft, P., & Paularena, K. I. (2002). Spatial Distribution of the Magnetosheath Ion Flux. *Advances in Space Research*, *30*(12), 2751–2756.

Palmaerts, B., Vogt, M. F., Krupp, N., Grodent, D., & Bonfond, B. (2017). Dawn-Dusk Asymmetries in Jupiter's Magnetosphere. In *Dawn-dusk asymmetries in planetary plasma environments* (pp. 307–322). American Geophysical Union (AGU). Retrieved from `https://agupubs.onlinelibrary.wiley.com/doi/abs/10.1002/9781119216346.ch24` doi: https://doi.org/10.1002/9781119216346.ch24

Palmroth, M., Ganse, U., Pfau-Kempf, Y., Battarbee, M., Turc, L., Brito, T., ... von Alfthan, S. (2018). Vlasov methods in space physics and astrophysics. *Living Reviews in Computational Astrophysics*, *4*(1), 1–54. Retrieved from `https://doi.org/10.1007/s41115-018-0003-2` doi: 10.1007/s41115-018-0003-2

Paularena, K. I., Richardson, J. D., Kolpak, M. A., Jackson, C. R., & Siscoe, G. L. (2001). A dawn-dusk density asymmetry in Earth's magnetosheath. *Journal of Geophysical Research: Space Physics*, *106*(A11), 25377–25394. doi: 10.1029/2000ja000177

Phillips, J. L., Luhmann, J. G., Knudsen, W. C., & Brace, L. H. (1988). Asymmetries in the Location of the Venus Ionopause. *Journal of Geophysical Research*, *93*(A5), 3927–3941.

Phillips, J. L., Luhmann, J. G., Russell, C. T., & Moore, K. R. (1987). Finite Larmor radius effect on ion pickup at Venus. *Journal of Geophysical Research*, *92*(A9), 9920. doi: 10.1029/ja092ia09p09920

Possolo, A., Merkatas, C., & Bodnar, O. (2019). Asymmetrical uncertainties.

Metrologia, *56*(4). doi: 10.1088/1681-7575/ab2a8d

Richardson, J. D. (2002). The magnetosheaths of the outer planets. *Planetary and Space Science*, *50*(5-6), 503–517. doi: 10.1016/S0032-0633(02)00029-6

Rojas Mata, S., & Futaana, Y. (2022). *Proton Plasma Bulk-Parameter Measurements in Venus' Dayside Magnetosheath.* Swedish National Data Service. doi: https://doi.org/10.5878/4wfd-pj36

Rojas Mata, S., Stenberg Wieser, G., Futaana, Y., Bader, A., Persson, M., Fedorov, A., & Zhang, T. (2022). Proton Temperature Anisotropies in the Venus Plasma Environment During Solar Minimum and Maximum. *Journal of Geophysical Research: Space Physics*, *127*(1). doi: 10.1029/2021JA029611

Romanelli, N., DiBraccio, G., Halekas, J., Dubinin, E., Gruesbeck, J., Espley, J., ... Luhmann, J. G. (2020). Variability of the Solar Wind Flow Asymmetry in the Martian Magnetosheath Observed by MAVEN. *Geophysical Research Letters*, *47*(22). doi: 10.1029/2020GL090793

Russell, C. T., Chou, E., Luhmann, J. G., Gazis, P. R., Brace, L. H., & Hoegy, W. R. (1988). Solar and interplanetary control of the location of the Venus bow shock. *Journal of Geophysical Research*, *93*(A6), 5461. doi: 10.1029/ja093ia06p05461

Schwartz, S. J., Burgess, D., & Moses, J. J. (1996). Low-frequency waves in the Earth's magnetosheath: present status. *Annales Geophysicae*, *14*(11), 1134–1150. doi: 10.1007/s00585-996-1134-z

Sheather, S. J. (2004). Density Estimation. *Statistical Science*, *19*(4), 588–597. doi: 10.1007/0-387-22732-6_5

Slavin, J. A., & Holzer, R. E. (1981). Solar wind flow about the terrestrial planets 1. Modeling bow shock position and shape. *Journal of Geophysical Research*, *86*(A13), 11401. doi: 10.1029/ja086ia13p11401

Soucek, J., Escoubet, C. P., & Grison, B. (2015). Magnetosheath plasma stability and ULF wave occurrence as a function of location in the magnetosheath and upstream bow shock parameters. *Journal of Geophysical Research: Space Physics*, *120*(4), 2838–2850. doi: 10.1002/2015JA021087

Soucek, J., Lucek, E., & Dandouras, I. (2008). Properties of magnetosheath mirror modes observed by Cluster and their response to changes in plasma parameters. *Journal of Geophysical Research*, *113*(A04203), 1–14. doi:

10.1029/2007JA012649

Spreiter, J. R., & Alksne, A. Y. (1966). Hydrodynamic flow around the magnetosphere. *Planetary and Space Science*, *14*, 223–253. Retrieved from https://doi.org/10.1016/0032-0633(66)90124-3. doi: 10.1016/0032-0633(66)90124-3

Spreiter, J. R., & Stahara, S. S. (1980). A new predictive model for determining solar wind-terrestrial planet interactions. *Journal of Geophysical Research*, *85*(A12), 6769. doi: 10.1029/ja085ia12p06769

Spreiter, J. R., & Stahara, S. S. (1994). Gasdynamic and magnetohydrodynamic modeling of the magnetosheath: A tutorial. *Advances in Space Research*, *14*(7), 5–19. doi: 10.1016/0273-1177(94)90042-6

Spreiter, J. R., Summers, A. L., & Rizzi, A. W. (1970). Solar Wind Flow past Nonmagnetic Planets – Venus and Mars. *Planetary and Space Science*, *18*, 1281–1299.

Stahara, S. S. (2002). Adventures in the magnetosheath: Two decades of modeling and planetary applications of the Spreiter magnetosheath model. *Planetary and Space Science*, *50*(5-6), 421–442. doi: 10.1016/S0032-0633(02)00023-5

Strangeway, R. J. (1991). Plasma waves at Venus. *Space Science Reviews*, *55*, 275–316. doi: 10.1007/BF00177139

Sundberg, T. (2017). Dawn-Dusk Asymmetries in Mercury's Magnetosphere. In *Dawn-dusk asymmetries in planetary plasma environments* (pp. 337–348). American Geophysical Union (AGU). Retrieved from https://agupubs.onlinelibrary.wiley.com/doi/abs/10.1002/9781119216346.ch26 doi: https://doi.org/10.1002/9781119216346.ch26

Svedhem, H., Titov, D. V., McCoy, D., Lebreton, J. P., Barabash, S., Bertaux, J. L., … Coradini, M. (2007). Venus Express - The first European mission to Venus. *Planetary and Space Science*, *55*(12), 1636–1652. doi: 10.1016/j.pss.2007.01.013

Titov, D. V., Svedhem, H., Koschny, D., Hoofs, R., Barabash, S., Bertaux, J. L., … Clochet, A. (2006). Venus Express science planning. *Planetary and Space Science*, *54*(13-14), 1279–1297. doi: 10.1016/j.pss.2006.04.017

Turc, L., Tarvus, V., Dimmock, A. P., Battarbee, M., Ganse, U., Johlander, A., … Palmroth, M. (2020). Asymmetries in the Earth's dayside magnetosheath:

Results from global hybrid-Vlasov simulations. *Annales Geophysicae*, *38*(5), 1045–1062. doi: 10.5194/angeo-38-1045-2020

Volwerk, M., Schmid, D., Tsurutani, B. T., Delva, M., Plaschke, F., Narita, Y., ... Glassmeier, K.-H. (2016). Mirror mode waves in Venus's magnetosheath: Solar minimum vs. solar maximum. *Annales Geophysicae*, *34*(11), 1099–1108. doi: 10.5194/angeo-34-1099-2016

Vörös, Z., Zhang, T., Leaner, M. P., Volwerk, M., Delva, M., & Baumjohann, W. (2008). Intermittent turbulence, noisy fluctuations, and wavy structures in the Venusian magnetosheath and wake. *Journal of Geophysical Research*, *113*, 1–11. doi: 10.1029/2008je003159

Walsh, A. P., Haaland, S., Forsyth, C., Keesee, A. M., Kissinger, J., Li, K., ... Taylor, M. G. (2014). Dawn-dusk asymmetries in the coupled solar wind-magnetosphere-ionosphere system: A review. *Annales Geophysicae*, *32*(7), 705–737. doi: 10.5194/angeo-32-705-2014

Walsh, B. M., Sibeck, D. G., Wang, Y., & Fairfield, D. H. (2012). Dawn-dusk asymmetries in the Earth's magnetosheath. *Journal of Geophysical Research: Space Physics*, *117*(12), 1–8. doi: 10.1029/2012JA018240

Wang, J., Xu, X., Yu, J., & Ye, Y. (2020). South-north asymmetry of proton density distribution in the Martian magnetosheath. *Earth and Planetary Physics*, *4*(1), 1–6. doi: 10.26464/epp2020003

Whittaker, I., Guymer, G., Grande, M., Pintér, B., Barabash, S., Federov, A., ... Bochsler, P. (2010). Venusian bow shock as seen by the ASPERA-4 ion instrument on Venus Express. *Journal of Geophysical Research: Space Physics*, *115*(9), 1–13. doi: 10.1029/2009JA014826

Xiao, S. D., & Zhang, T. (2018). Solar cycle variation of the venus magnetic barrier. *Planetary and Space Science*, *158*(April), 53–62. Retrieved from `https://doi.org/10.1016/j.pss.2018.05.006` doi: 10.1016/j.pss.2018.05.006

Xiao, S. D., Zhang, T., & Vörös, Z. (2018). Magnetic Fluctuations and Turbulence in the Venusian Magnetosheath Downstream of Different Types of Bow Shock. *Journal of Geophysical Research: Space Physics*, *123*(10), 8219–8226. doi: 10.1029/2018JA025250

Zhang, T., Baumjohann, W., Delva, M., Auster, H.-U., Balogh, A., Russell, C. T., ... Lebreton, J.-P. (2006). Magnetic field investigation of the Venus plasma environment: Expected new results from Venus Express. *Planetary and Space Science*, *54*(13), 1336–1343. Retrieved from `https://www.sciencedirect.com/science/article/pii/S0032063306001607` doi: https://doi.org/10.1016/j.pss.2006.04.018

Zhang, T., Baumjohann, W., Du, J., Nakamura, R., Jarvinen, R., Kallio, E., . . . Russell, C. T. (2010). Hemispheric asymmetry of the magnetic field wrapping pattern in the Venusian magnetotail. *Geophysical Research Letters*, *37*(14). doi: 10.1029/2010GL044020

Zhang, T., Luhmann, J. G., & Russell, C. T. (1991). The Magnetic Barrier at Venus. *Journal of Geophysical Research: Space Physics*, *96*(A7), 11145–11153.

Zhang, T., Schwingenschuh, K., Russell, C. T., & Luhmann, J. G. (1991). Asymmetries in the Location of the Venus and Mars Bow Shock. *Geophysical Research Letters*, *18*(2), 127–129.